Earthquakes and Structures, *Vol. 14, No. 6 (2018) 551-565*
DOI: https://doi.org/10.12989/eas.2018.14.6.551

Performance analysis of a detailed FE modelling strategy to simulate the behaviour of masonry-infilled RC frames under cyclic loading

Hossameldeen M. Mohamed[1,2a] and Xavier Romão[*1]

[1]*CONSTRUCT-LESE, Faculty of Engineering, University of Porto, Rua Dr. Roberto Frias, 4200-465 Porto, Portugal*
[2]*Department of Civil Engineering, Faculty of Engineering, Aswan University, Abo El-Reesh Mail Box NO.: 81542, Aswan, Egypt*

(Received February 23, 2017, Revised April 6, 2018, Accepted April 10, 2018)

Abstract. Experimental testing is considered the most realistic approach to obtain a detailed representation of the nonlinear behaviour of masonry-infilled reinforced concrete (RC) structures. Among other applications, these tests can be used to calibrate the properties of numerical models such as simplified macro-models (e.g., strut-type models) representing the masonry infill behaviour. Since the significant cost of experimental tests limits their widespread use, alternative approaches need to be established to obtain adequate data to validate the referred simplified models. The proposed paper introduces a detailed finite element modelling strategy that can be used as an alternative to experimental tests to represent the behaviour of masonry-infilled RC frames under earthquake loading. Several examples of RC infilled frames with different infill configurations and properties subjected to cyclic loading are analysed using the proposed modelling approach. The comparison between numerical and experimental results shows that the numerical models capture the overall nonlinear behaviour of the physical specimens with adequate accuracy, predicting their monotonic stiffness, strength and several failure mechanisms.

Keywords: masonry infill; reinforced concrete structure; finite element model; ANSYS; cyclic loading

1. Introduction

Reinforced concrete (RC) frames with masonry infills are one of the most common structural systems in the world, even in earthquake-prone regions. However, the severe human and economic losses that occurred in masonry-infilled RC structures in recent earthquakes, e.g., Kocaeli, Turkey, 1999 (Sezen *et al*. 2003), L'Aquila, Italy, 2009 (Ricci *et al*. 2011), Tabanlı (Van), Turkey, 2011 (Tapan *et al*. 2013), or Lorca, Spain, 2011 (De Luca *et al*. 2014), clearly show the vulnerability of these structures. Therefore, adequate seismic vulnerability studies need to be carried out in order to foresee the performance of these structures and establish effective strengthening strategies where needed. Since these seismic vulnerability studies usually require a large number of analyses (Vamvatsikos and Cornell 2002, Ibrahim and El-Shami 2011, Baker 2015), the use of simplified macro-modelling approaches to represent the behaviour of infill panels under earthquake loading has been shown to provide adequate results while reducing the level of computational effort required (Uva *et al*. 2012). Still, to obtain realistic results, the mechanical properties of these simplified macro-models need to be calibrated, usually using available experimental data (El-Dakhakhni *et al*. 2003). However, due to the variability of existing masonry infill types across countries (i.e., involving variable configurations, as well as different construction technologies and materials), the available experimental data do not cover all these possibilities and requirements. Since carrying out experimental tests commonly requires a significant amount of resources, alternative approaches need to be established to obtain adequate data at a lower cost to calibrate the referred simplified macro-models.

In light of this, the use of adequate detailed finite element (FE) models that are able to represent the complex behaviour of RC masonry-infilled structures is proposed herein for cases where experimental data are not available or experimental tests are unable to be carried out. In this context, the current article proposes a detailed FE modelling approach that is able to reproduce the most important features of the in-plane behaviour of RC masonry-infilled frames under monotonic and cyclic loading. By using this modelling approach, a realistic simulation of the masonry infill behaviour is achieved. One of the outputs of the analysis is a reliable capacity curve of the masonry infilled RC frame that can then be used to calibrate the properties of simplified macro-models. The proposed modelling strategy does not involve the development of new constitutive laws or FE formulations. Instead, it explores the capabilities of the commercial software ANSYS to model this type of structure at an affordable cost. By doing so, the selected approach can also be more easily replicated by other researchers. After presenting the characteristics and features of the proposed approach, the results of several experimental tests are simulated to validate this numerical strategy.

*Corresponding author, Assistant Professor
E-mail: xnr@fe.up.pt
[a]Assistant Professor
E-mail: Hossam.ahmed@aswu.edu.eg

ISSN: 2092-7614 (Print), 2092-7622 (Online)

2. Detailed FE modelling of RC masonry-infilled structures

2.1 Existing research

Due to the difficulties and the costs associated with the experimental testing of masonry-infilled RC structures, a significant amount of research has been carried out over the past 20 years to analyse the behaviour of these structures using detailed FE models, e.g., see the review in (Asteris *et al*. 2013, Tarque *et al*. 2015). These studies attempted to represent the behaviour of the RC frame and of the infill wall using different strategies and achieved different levels of accuracy. One of the earliest finite element models analysing the behaviour of masonry-infilled RC structures was presented in (Mehrabi and Shing 1997). Even though this approach was able to achieve an adequate match of the experimental data, the behaviour of the model under cyclic loading was not examined. Stavridis and Shing (2010), Koutromanos *et al*. (2011) also developed a complex nonlinear finite element model for masonry-infilled RC structures that combined the smeared (for masonry units) and discrete crack (for mortar joints) modelling approaches for the infill and discretised the RC columns into several elements in order to capture their potential shear failure. Despite its accuracy, this model was found to be computationally intensive, as referred by Sattar (2013), who developed a continuum FE model involving less computational effort using the software DIANA (DIANA 2011). This model was able to provide a good agreement with experimental data for monotonic loading even though it was not developed such as to capture the potential shear failure of columns and the discrete cracking in masonry units. Furthermore, the performance of this model was also not examined for cyclic loading.

In the context of using commercial software for this type of analysis, aside from the software DIANA, the software ANSYS (ANSYS 2012) has also been used by several researchers to develop detailed FE models of RC infilled structures and determine their behaviour. These studies adopted different strategies to model the RC and the infill components in terms of the level of refinement. For example, Mohyeddin *et al*. (2013a) developed a refined FE model to analyse the monotonic behaviour of RC frames with infills. However, in order to achieve more stable numerical analyses and avoid excessive deformation of the masonry FE units, part of the mortar elements adjacent to the contact elements are assumed to be linear elastic. Alam *et al*. (2009), Noorfard and Marefat (2009) also developed refined models in ANSYS for this type of structure using homogeneous continuum elements. In their approaches, the masonry was modelled using four-node plane stress elements and the mortar behaviour was simulated using a surface-based cohesive contact model to capture the cracking and sliding failure of the mortar joints. Although using homogeneous continuum elements to model the infills, they obtained a reasonable agreement between the numerical results and the experimental data for the global monotonic loading analyses. Still, these models do not account for the crushing or the cracking that may occur in the masonry units. A similar modelling approach was also used by Wael and Drysdale (2004) and Chen and Liu (2016) to simulate the behaviour of steel frames with masonry infills and numerical results with the same type of quality were also obtained.

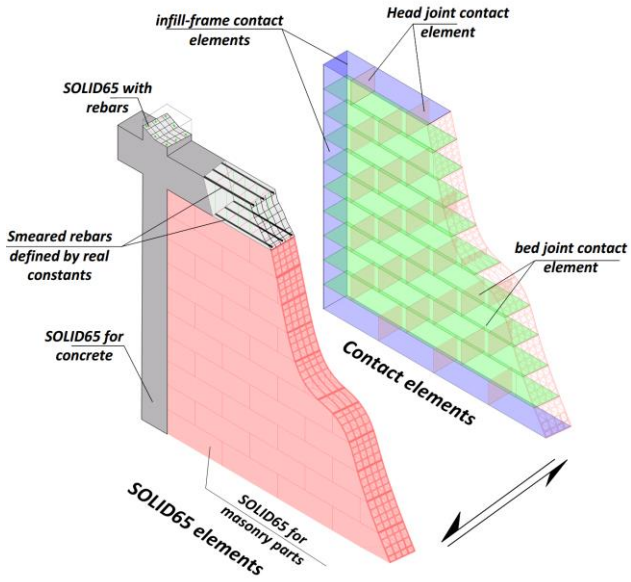

Fig. 1 General schematics of the refined FE model for masonry-infilled RC frames.

2.2 Proposed FE modelling approach

Although the use of refined modelling approaches is found to be computationally intensive and unsuited for practical performance based earthquake engineering applications where multiple analyses need to be carried out, their use is believed to be a potential alternative to experimental testing. Therefore, the objective of the proposed modelling approach is to allow the development of numerical models balanced in terms of modelling detail and computational cost that will provide reliable data to calibrate the parameters of simplified models representing the behaviour of infills under earthquake loading. Consequently, the characteristics of the finite element modelling strategy were selected in order to capture the various failure mechanisms that masonry infill panels may exhibit under both monotonic and cyclic loading conditions. The modelling strategy is able to capture shear sliding along the mortar joints, tensile cracking and compressive crushing of the mortar joints and bricks, and the general mechanism of force transfer between the infill and the surrounding frame. As such, this modelling approach is able to overcome some of the limitations of previous studies developed with the software ANSYS.

To illustrate the proposed nonlinear finite element modelling approach, Fig. 1 shows the schematics of the finite element mesh components for a one-bay and one storey masonry-infilled RC frame, termed specimen M2 (Pires 1990), that will be used in a subsequent section to analyse the performance of the proposed modelling approach. The RC and masonry components are modelled using the eight-node hexahedral solid FE termed SOLID65

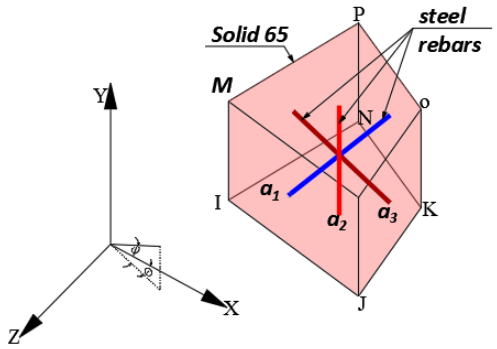

Fig. 2 General schematics of the SOLID65 FE with the capability to accommodate three rebars in three directions using the real constants option

and available in ANSYS (Release 14.0) (ANSYS 2012). The cross sections of the beams, columns and their connections are meshed using this FE and the longitudinal reinforcement rebars are merged with a limited number of elements according to the actual rebar locations (rebars are assigned to the solid FE as additional properties using the software ANSYS option known as "real constants"). Up to three rebar materials can be assigned to the element SOLID65. Rebar specifications include the material number, the volume ratio, and the orientation angles as shown in Fig. 2. The masonry brick units (i.e., the brick blocks) are modelled according to their real geometry, i.e., including the voids of the hollow brick units, to represent the contact between surfaces and the fragility of the brick units more realistically. In order to represent the interaction between different brick units and their interaction with the surrounding RC frame, contact elements (CONTA174 and TARGE170 available in ANSYS) were combined with a cohesive zone material (CZM) model using different parameters to accommodate different joint situations. To reduce the number of interface elements needed and the computational costs, the thickness of the mortar joints was divided in two parts that were connected to the adjacent masonry units, using a discretization approach of the masonry components similar to that of (Lourenço and Rots 1997) but using the CZM model to control the tensile separation and the shear sliding between these components. The interaction between the two parts of the mortar joint (and their adjacent masonry units) is then defined by the properties of the contact elements.

The ability of element SOLID65 to represent both materials of RC members (i.e., steel and concrete) reduced the number of element typologies that were needed in the modelling (i.e., there was no need to use a separate element for the steel rebars such as a link element). Ultimately, this modelling approach also reduced the level of computational effort that was required. Furthermore, by using contact elements with the CZM model, several aspects of the complex interaction between the masonry infill and the RC frame are able to be captured by the numerical model. Given its characteristics, the proposed modelling approach is able to capture the more common failure mechanisms of masonry infills (e.g., crushing and tensile fracture of the masonry, cracking and shear slipping at the masonry interfaces (Shing and Mehrabi 2002)). Furthermore, when cracking or shear slipping occurs at a masonry interface, the model is also able to account for the discrete behaviour of the post-failure interface system. On the other hand, when the crushing or tensile fracture of a masonry unit occurs, the post-failure separation/splitting of the brick into discrete blocks is not accounted in order to reduce the computational effort. The proposed modelling approach is also able to represent flexural failure modes of the RC elements but does not account for the possible shear failure of these elements. In this context, it is noted that the main purpose of the numerical model is not to represent the behaviour of the masonry-infilled RC frame system, but to characterize the behaviour of the masonry infill while accounting for the influence of the surrounding RC frame. Therefore, the inability to capture the shear failure of RC elements is not seen to be particularly important. Finally, it is noted that ANSYS has limited modelling capabilities to represent the cyclic degradation of materials. Therefore, cyclic degradation effects resulting in unloading/reloading stiffness degradation, strength degradation or pinching effects are only able to be represented in a simplified way.

2.2.1 Material modelling of the concrete

The concrete material model CONCR available in ANSYS was combined with the SOLID65 element to represent the behaviour of the concrete due to its ability to represent cracking in tension and crushing in compression. The CONCR material model requires the definition of four parameters: the β_t and β_c shear coefficients, the concrete tensile strength f_t and the concrete compressive strength f_c. Parameters β_t and β_c control the amount of shear that is transferred across an opened and closed crack, respectively, and their values range from 0 to 1 (Kwan *et al.* 1999), where 0 represents a smooth crack (i.e., with total loss of shear transfer) and 1 represents an irregular crack (i.e., with no loss of shear transfer). The occurrence of numerical convergence problems was reported in (Vijaya *et al.* 2014) when parameter β_t is lower than 0.20 and no significant changes in the response were found as a result of using different values of this parameter. Therefore, in the present study, parameter β_t was set to 0.40 and parameter β_c was set to 0.80 (Xiaohan and Xilin 1996). The CONCR material model follows the failure surface proposed in (William and Warnke, 1975) where the material behaves linearly until crushing or cracking. The tensile behaviour follows the stress-stain relation shown in Fig. 3 where E is the modulus of elasticity of the concrete defined according to the behaviour in compression.

Since the CONCR material model behaves as a linear elastic material in compression, it was combined with a nonlinear model in order to produce a realistic nonlinear stress–strain relation. The constitutive model proposed in (Kent and Park 1971) known as the "Kent-Park model" and its modified version (Scott *et al.* 1982) are used to define the envelope curves for the unconfined and confined concrete hysteretic behaviour in compression, respectively. These models are known to exhibit a good agreement with experimental results (Scott *et al.* 1982, Mohyeddin *et al.* 2013b) and provide a good balance between simplicity and accuracy (Taucer *et al.* 1991). The Kent-Park model was

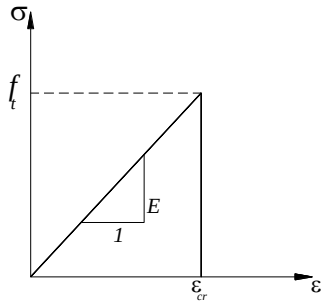

Fig. 3 Stress-strain curve of the CONCR material model in tension (ANSYS 2012)

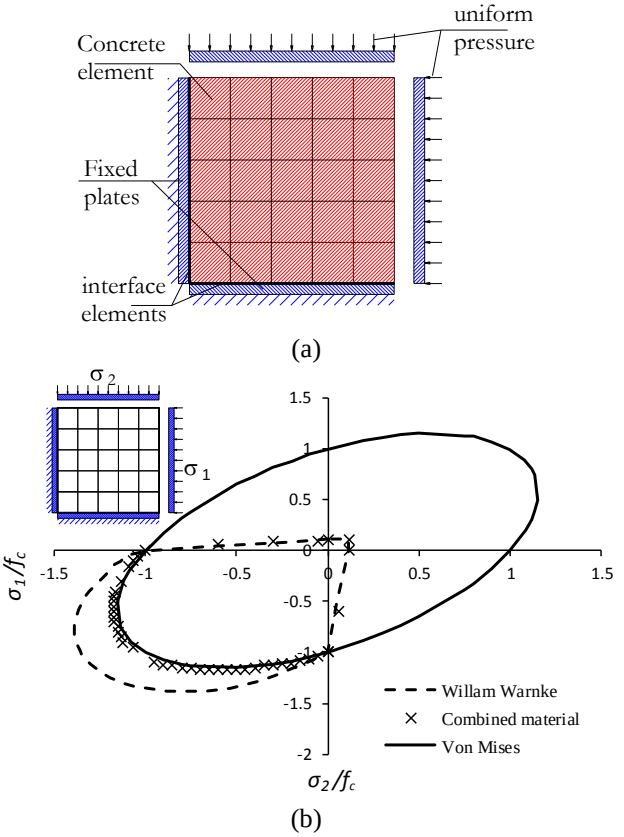

Fig. 4 (a) Biaxial loading test structure, (b) A comparison between the Von Mises and Willam Warnke failure surfaces with the combined material failure surface which is used to represent concrete material

used to define a multi-kinematic material model MKIN for the concrete behaviour in compression with the crushing capability of the SOLID65 element deactivated to avoid the premature failure of the concrete (Chansawat, *et al*. 2001) and to guarantee that the concrete element follows the selected constitutive model. The Poisson ratio is considered to be 0.20 and the modulus of elasticity E is defined according to the Kent-Park constitutive model.

In order to validate the behaviour of this combined material model, the structural model shown in Fig. 4(a) was tested. The structure is a unit cube made of concrete SOLID65 elements with characteristics from (Kakaletsis and Karayannis 2009) connected to interface elements supported by two fixed plates. This structure was subjected

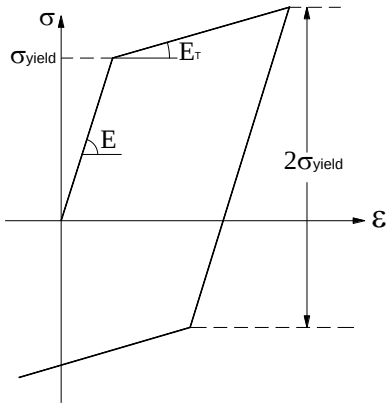

Fig. 5 Bilinear steel stress-strain curve with Bauschinger effect

to incremental uniform pressures in both the X and Y directions until failure in order to trace the failure surface of the combined material. The failure surface produced from that numerical test is shown in Fig. 4(b) along with the Willam Warnke and the Von Mises failure surfaces (Mises 1913). Fig. 4(b) shows that the failure surface of the combined material matches the Willam Warnke failure surface in all the stress domains except in the compression-compression domain where it matches the Von Mises failure surface. This is caused by the deactivation of a parameter of the CONCR material model which switches the behaviour of the concrete in that domain to the multi-kinematic hardening material that follows the Von Mises failure surface.

2.2.2 Material modelling of the steel reinforcement

In this study, the steel behaviour was represented by a bilinear stress-strain relation. As shown in Fig. 5, the bilinear material is defined by the value of the yield stress σ_{yield} and of the post-yield tangent modulus E_T. This material exhibits kinematic hardening accounting for the Bauschinger effect (Hu *et al*. 2016) for cyclic loading, as shown in Fig. 5. If experimental data about the post-yield behaviour of steel is unavailable, E_T is assumed to be equal to 2.5% of the initial modulus of elasticity (Mohyeddin *et al*. 2013a). The Poisson ratio of the steel material is considered to be 0.30.

2.2.3 Material modelling of the masonry brick units

The modelling approach selected for the concrete is also used to model the masonry units. Therefore, all the details provided for the concrete material modelling in terms of tensile behaviour and failure surface are also applicable to the modelling strategy that was selected for the masonry units. The following nonlinear stress–strain curve from (Angel 1994) is adopted for the compression stress state of the masonry material

$$\sigma_m = \frac{27 f'_{cm}\left(250\varepsilon_{crm}-1\right)}{4\varepsilon_{crm}^3}\varepsilon_m^3 + \frac{27 f'_{cm}\left(1-333.33\varepsilon_{crm}\right)}{4\varepsilon_{crm}^3}\varepsilon_m^3 + E_m\varepsilon_m \quad (1)$$

where ε_m and σ_m are the compressive strain and the corresponding compressive stress of the masonry, respectively, $f_{cm}^{'}$ is the maximum compressive strength of the masonry, ε_{crm} is the compressive strain at the onset of failure and E_m is the modulus of elasticity given by

$$E_m = 750 f_{cm}^{'} \tag{2}$$

It is noted that the second derivative of Eq. (1) is only negative as long as ε_{crm} is within 0.003~0.0048; otherwise a positive value is obtained which leads to a situation where it is not possible to match the behaviour of the expression with experimental data. For larger values of ε_{crm}, the following expression proposed in (Hendry 1990) is suggested as an alternative model for the compression stress state of the masonry material

$$\sigma_m = f_{cm}^{'}\left[2\frac{\varepsilon_m}{\varepsilon_{crm}} - \left(\frac{\varepsilon_m}{\varepsilon_{crm}}\right)^2\right] \tag{3}$$

In this study, both Eq. (1) and Eq. (3) were used, depending on the characteristics of the masonry of the specimen under analysis (i.e., ε_{crm}). With respect to the tensile behaviour, if experimental data for the tensile strength of the masonry units are unavailable, its value is set as 10% of the compressive strength, as suggested in (Crisafulli 1997). Based on (Anthoine 1992), the Poisson ratio for masonry is considered to be 0.19.

2.2.4 Modelling of the interface elements

The surface contact pair elements CONTA174 and TARGE170 are used to represent the interaction between the masonry units and between the masonry infill and the RC frame. To model the separation and the slip of the contact surfaces, the CZM model is assigned to these contact elements along with a friction material model. Generally, the CZM model involves a constitutive relation between traction stresses acting at the interface, either in shear or in tension, and the corresponding interface slip or separation δ. According to this model, the contact pair is connected until the contact displacement exceeds the maximum separation/slip value $\delta_{\max}$, as shown in Fig. 6(a). Before $\delta_{\max}$ occurs, the contact elements behave according to one of the considered bilinear CZM models that are used to account for debonding in tension (mode I) and in shear (mode II), Figs. 6(b) and (c), respectively (Alfano and Crisfield 2001). The bilinear relation between the traction stress and its corresponding traction distance δ can be defined by the maximum stress and the maximum traction distance or, alternatively, by the maximum traction stress and the corresponding fracture energy (Alfano *et al.* 2001, Mohyeddin *et al.* 2013b). In the current modelling approach, the input parameters that were selected to define the CZM are the maximum normal contact stress $\sigma_{\max}$ and the contact separation at full debonding δ_n^c for mode I, and the maximum equivalent tangential contact stress $\tau_{\max}$ and the tangential slip at full debonding δ_s^c for mode II.

The tensile debonding parameters were defined in order to represent the tensile behaviour of mortar. As such, the maximum normal contact stress $\sigma_{\max}$ is considered to be

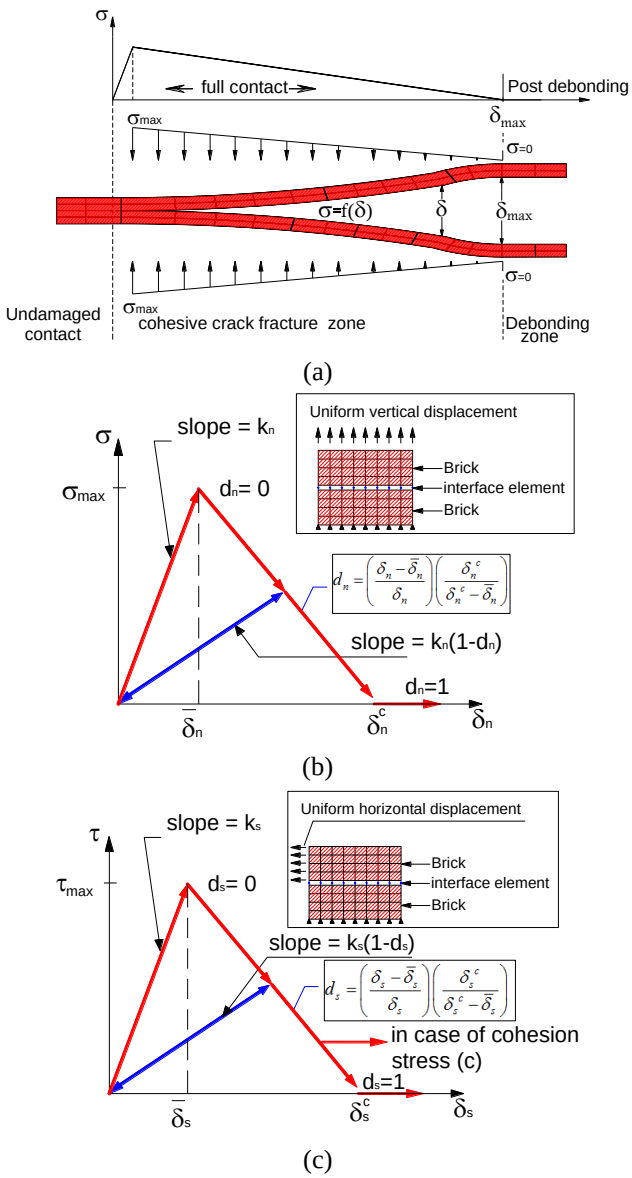

Fig. 6 (a) Definition of the CZM model; (b) bilinear definition of the CZM for tensile debonding (mode I) (c) bilinear definition of the CZM for shear debonding (mode II)

equal to the tensile strength of the mortar and the maximum normal contact gap δ_n^c is assumed to be six times the value of $\bar{\delta}_n$, the displacement corresponding to $\sigma_{\max}$ (Induprabha and Dilrukshi 2011). For the shear debonding behaviour, the maximum equivalent tangential contact stress $\tau_{\max}$ was defined according to available experimental results, while the tangential slip at full debonding δ_s^c was assumed to be within 2-3 mm (Lourenço *et al.* 2004). In order to accommodate cases of partial joint filling or inferior quality conditions of the head joints and horizontal joints between the infill panel and the RC beam of the frame, the cohesion stress between the contact pair was ignored for the contact between the masonry and the surrounding RC frame. In addition, the debonding stresses in these joints were also reduced to seventy percent of the value for the bed joints

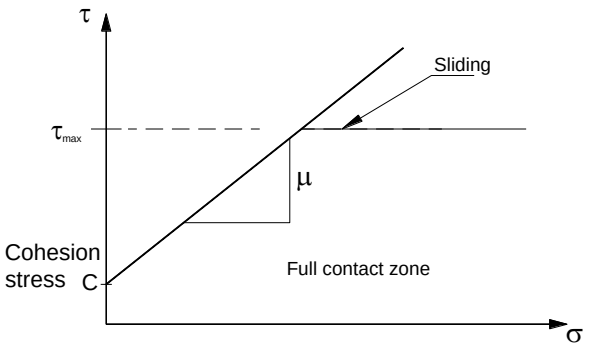

Fig. 7 Behaviour of the contact element after full debonding according to Coulomb's friction law

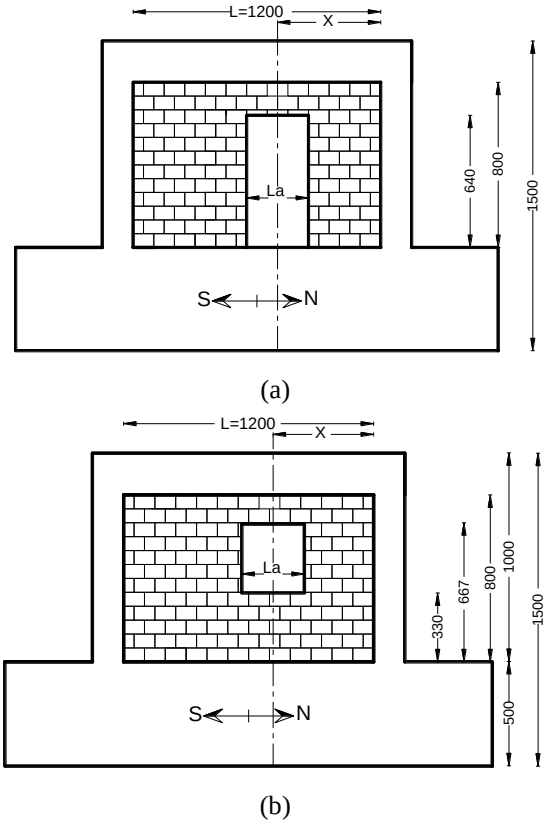

Fig. 8 Description of the partially infilled specimens: (a) specimens with door openings; (b) specimens with window openings (Kakaletsis *et al*. 2008, Kakaletsis *et al*. 2009, Kakaletsis 2009) (All dimensions are in millimetre)

(Mohyeddin *et al*. 2013a).

After full debonding, the surface interaction is governed by standard contact constraints for the normal and tangential directions. For normal stresses, these constraints establish that only compression stress is transferred through the contact pair. For the case of tangential stresses, these are transferred according to the classical Coulomb friction law, as shown in Fig. 7 where μ is the friction coefficient. For bed joints, the value of μ is based on available experimental results or considered to be 0.77 otherwise. The value of μ for head joints and between the masonry infills and the surrounding RC frame was defined as sixty percent of the value considered for bed joints to accommodate partial joint

Table 1 Characteristics of the test specimens with partially infilled RC frames (Kakaletsis *et al*. 2008, Kakaletsis *et al*. 2009, Kakaletsis 2009)

Specimen description	Opening type		Opening size *La/L*
	Window	Door	
Centered window	√		0.25
Centered window	√		0.375
Non-centered window	√		0.50
Non-centered window	√		0.25
Non-centered window	√		0.25
Centered door		√	0.25
Non-centered door		√	0.25
Non-centered door		√	0.25

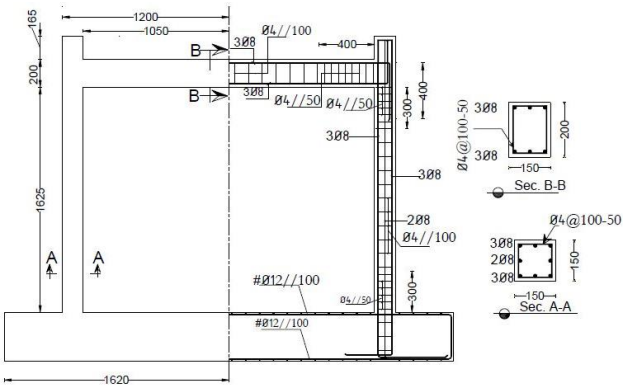

Fig. 9 Geometry and reinforcement details of specimen M1 (Pires 1990) (a) and of specimen B (Kakaletsis *et al*. 2008, Kakaletsis *et al*. 2009, Kakaletsis 2009) (All dimensions are in millimetre)

filling and the inferior quality conditions of these joints (Mohyeddin *et al*. 2013a).

3. Experimental data selected for the validation of the proposed modelling approach

A set of specimens from two different experimental campaigns (Pires 1990, Kakaletsis and Karayannis 2008, Kakaletsis *et al*. 2009, Kakaletsis 2009) were selected to validate the detailed numerical models. The selected data

Table 2 Mechanical properties of the materials involved in the experimental specimens

Specimen ID	Concrete		Steel reinforcement			Infill panel		Vertical loading (kN)
	f_c (MPa)	f_t (MPa)	Size (mm)	σ_{yield} (MPa)	σ_{ultimate} (MPa)	Brick unit f_m (MPa)	Mortar f_{mo} (MPa)	
M	(24.6*, 33.1**)[1]	n/a	Ø 8	434.3	519.3	--	--	200
M2	(23.5*, 28.3**)[1]	n/a	Ø 4	522.7	552.3	4.80	6.2*,6.4**	220
B[2]	28.5	n/a	Ø 5.6	390.5	516.3	--	--	100
S[2]	28.5	n/a	Ø 3	212.2	321.1	3.10	1.53	100

- f_c is the compressive strength of concrete, f_t is the tensile strength of concrete, σ_{yield} is the steel yield stress and σ_{ultimate} is the ultimate strength of steel

[1] cubic strength which was converted to cylinder strength.

[2] the rest of the specimens from this test campaign have the same mechanical properties

* at 28 days, ** when the specimen was tested

- the brick unit used in specimen M2 has dimensions of 200*150*300 mm^3 and the dimensions of the brick unit used in specimens from (Kakaletsis *et al*. 2008, Kakaletsis *et al*. 2009, Kakaletsis 2009) are 60*60*93 mm^3

- For the masonry material of specimen M2, ε_{crm} is 0.0048, while for the rest of the specimens, ε_{crm} is 0.006

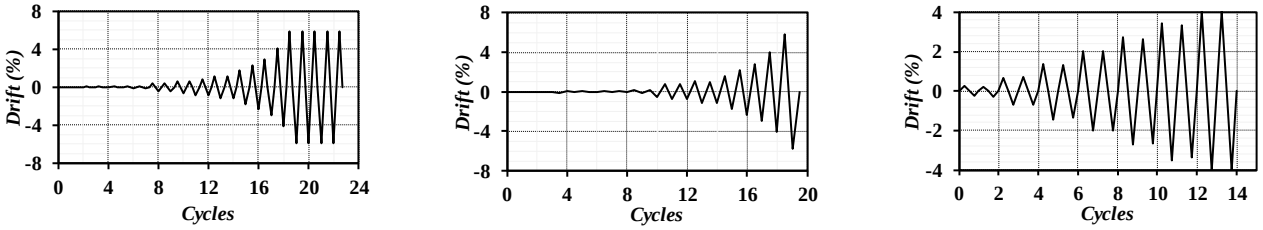

(a) (b) (c)

Fig. 10 Cyclic displacement evolutions defining the loading considered for specimen M1 (a), for specimen M2 (b) and for specimens B, S and all the partially infilled frames

are those from specimens M1 and M2 from (Pires 1990) and specimens B, S, DO2, DX1, DX2, WO4, WO3, WO2, WX2 and WX1 from (Kakaletsis *et al*. 2008, Kakaletsis *et al*. 2009, Kakaletsis 2009). The specimens were tested under increasing cyclic lateral loading. The common aspect between these tests is that all specimens were scaled models and are one-bay one-storey frames.

Specimens M1 and B are bare RC frame specimens, specimens M2 and S are fully infilled RC frames, and the remaining specimens (DO2, DX1, DX2, WO4, WO3, WO2, WX2, and WX1) are partially infilled RC frames with various configurations as shown in Fig. 8 and Table 1. The geometric description of the RC frames of specimens M1 and B along with their reinforcement detailing are shown in Fig. 9. It is noted that the RC frame of the masonry infilled specimens of a given test campaign has a configuration identical to that of the corresponding bare frame. The average mechanical properties of the materials involved in these specimens are summarized in Table 2. With respect to these properties, the significant difference between the relative strengths of the brick units and mortar of specimens M2 and S should be noted. Furthermore, it is also noted that the brick units used in the test of specimen M2 were real size (unscaled) brick units.

With respect to the numerical modelling, it is referred that, in order to reduce the size of the models, the base of the columns was considered as fixed points instead of modelling the real base of the experimental specimens (e.g., with a beam or slab). The compressive behaviour of the masonry units was modelled using Eq. (3) for specimen M2 and using Eq. (1) for the remaining specimens. Due to length restrictions, a detailed description of all the parameters involved in the simulations performed in the software ANSYS cannot be presented herein. Still, all the necessary details are provided in (Mohamed 2017). Furthermore, the cyclic loading that was applied to each specimen corresponds to the cyclic lateral displacement loading histories considered in the experimental tests and represented in Fig. 10. It is noted that the displacement loading histories considered in the simulations are not exactly the ones applied in the experimental tests. Since the experimental displacement histories exhibited variable displacement increments, the displacement increments of the numerical loading histories were made more uniform. Furthermore, the size of the displacement increments was reduced sometimes also during the numerical analyses to facilitate numerical convergence.

4. Validation of the proposed refined FE modelling approach

4.1 Analysis of the RC bare frames

To validate the modelling approach selected for the RC members, the experimental cyclic lateral loading tests carried out in the two bare frame specimens (specimens M1 and B) were simulated numerically. Before applying the lateral displacement loading history, the experimental vertical loads were applied. To illustrate the performance of

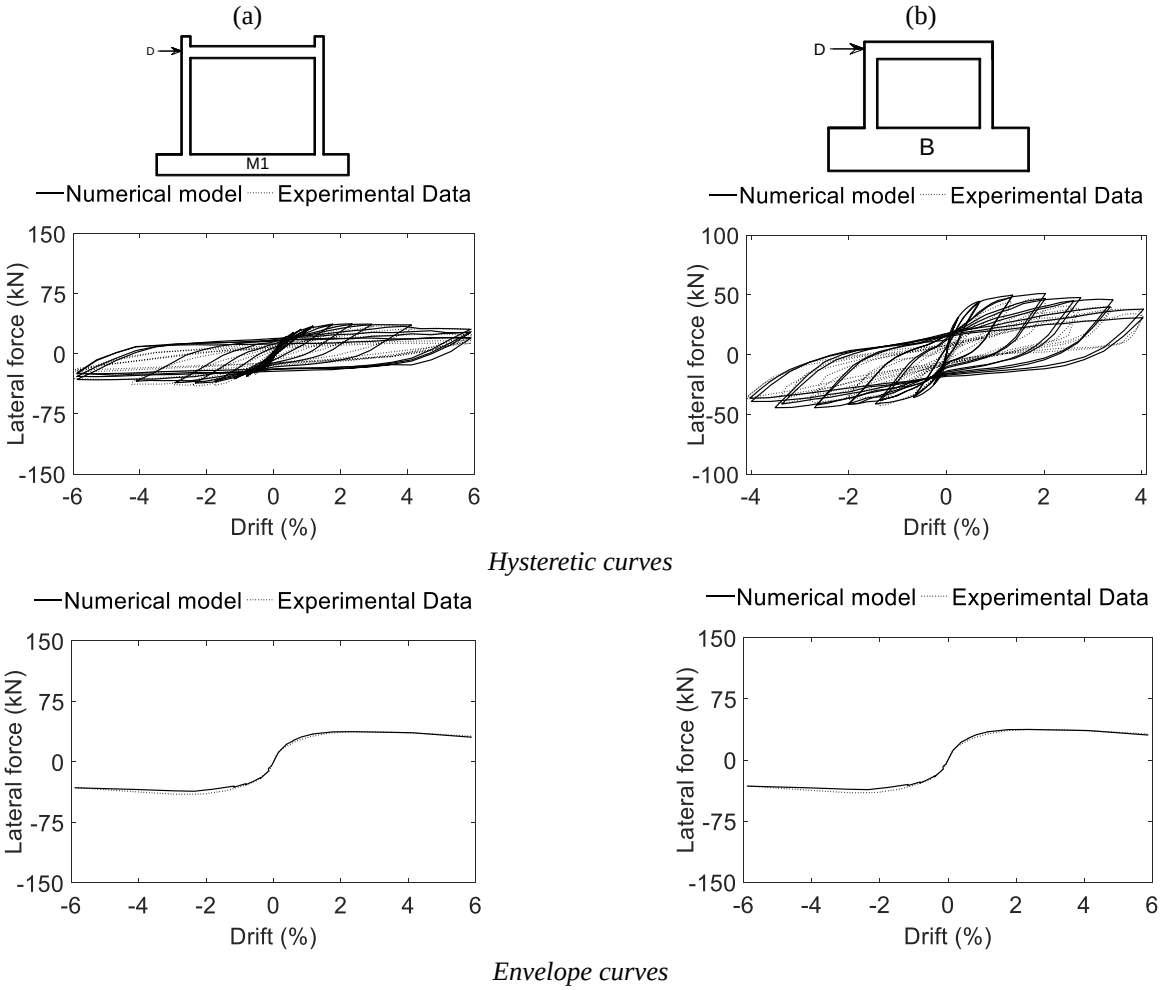

Fig. 11 Load–deflection curves obtained from the experimental tests and from the numerical models: (a) specimen M1; (b) specimen B

the numerical model, Figs. 11(a) and (b) compare the experimental lateral load-deflection curves for specimens M1 and B, respectively, with those that were obtained from the numerical analyses. To provide a better analysis of the level of lateral deflection involved in the tests, this parameter is represented in terms of lateral drifts. Furthermore, to increase the readability of the results, both the full cyclic lateral load-deflection curves and the overall envelope curves are shown for both frames. The results indicate that the numerical models are able to adequately match the experimental cyclic response. However, when the lateral drift exceeds 2.5%, the numerical unloading/ reloading branches deviate slightly from the experimental results. These differences are due to the unloading and reloading stiffnesses associated to the model representing the concrete compressive behaviour which is unable to represent cyclic degradation effects, i.e., the unloading and reloading stiffnesses are always equal to the initial stiffness. To complement these results, Fig. 12 compares the crack patterns of specimen M1 and specimen B obtained from the numerical analyses with those obtained experimentally. It can be seen that the numerical models are able to capture the overall crack propagation in the columns and the beam for both specimens. Still, for the case of specimen B, the

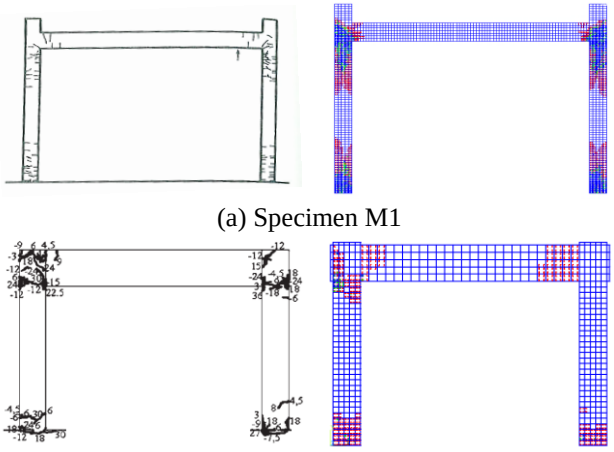

(a) Specimen M1

(b) Specimen B

Fig. 12 Experimental and numerical crack patterns: a) specimen M1; b) specimen B.

crack pattern in the right upper corner was not adequately captured. From the numerical point of view, the referred limitations associated to the model representing the cyclic behaviour of concrete might play a role in these differences. Aspects related to the experimental test itself cannot be

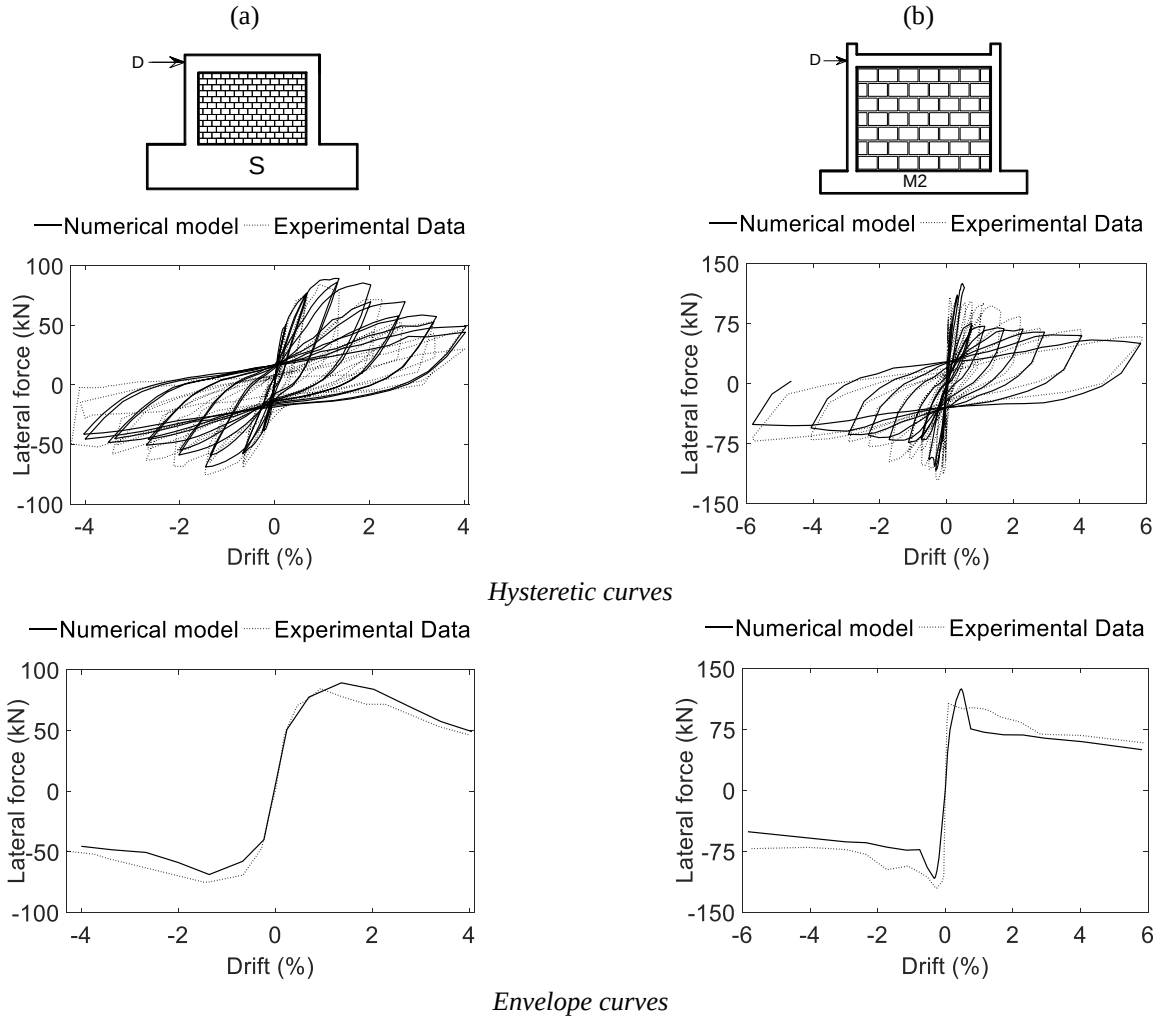

Fig. 13 Load–deflection curves obtained from the experimental tests and from the numerical models: (a) specimen S (b) specimen M2

discarded also, particularly since the experimental crack pattern is also asymmetric. However, since detailed information on the experimental tests is not available, it is not possible to obtain further insights about these differences.

4.2 Analysis of the RC fully infilled frames

Two different specimens with fully infilled RC frames were analysed using the referred numerical models for the RC frame and the infill panel. As for the bare frames, the experimental vertical loads were applied before applying the lateral displacement loading history. To demonstrate the performance of the numerical model, Figs. 13(a) and (b) compare the experimental lateral load-deflection curves for specimens S and M2, respectively, with those that were obtained from the numerical analyses. As for the bare frames, the lateral deflection is represented in terms of drifts and both the full cyclic lateral load-deflection curves and the overall envelope curves are shown for both frames. The figures show a reasonable agreement between experimental results and those obtained from the developed micro-modelling approach, particularly in terms of the global behaviour (stiffness and strength). However, as for the bare frames, the unloading/reloading stiffness of the numerical results deviates from the experimental one for larger drifts (i.e., when it exceeds a drift around 2.5%) which is due to the factors referred in the previous section. The larger differences found between the numerical and experimental behaviour of specimen M2 are assigned to an experimental factor that was not able to be accounted for in the numerical model. During the experimental test, a horizontal crack was developed between the 5^{th} and 6^{th} masonry courses for a lateral drift of 0.14% (a low level of drift), (Pires 1990). The development of this crack and the subsequent debonding of the interface changed the load transfer mechanism of the infill panel and delayed the post-peak strength degradation of the infill due to crack propagation effects. It is assumed that this occurred in the physical specimen due to a lower quality of the mortar between the referred masonry courses. This weaker mortar layer and its post-failure frictional behaviour were not accounted for in the numerical modelling since no data was available (e.g., the strength of that weaker mortar) to represent that experimental behaviour. Furthermore, simulating this experimental test under these conditions emphasizes the performance of the numerical model when unforeseen

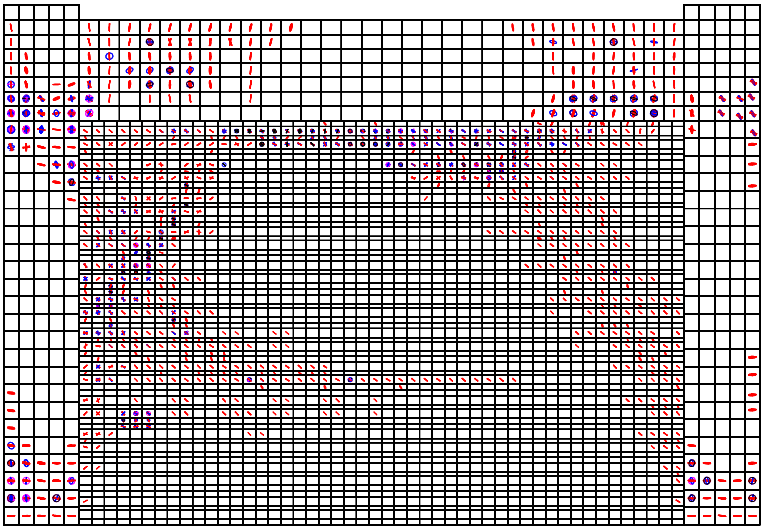

(a)

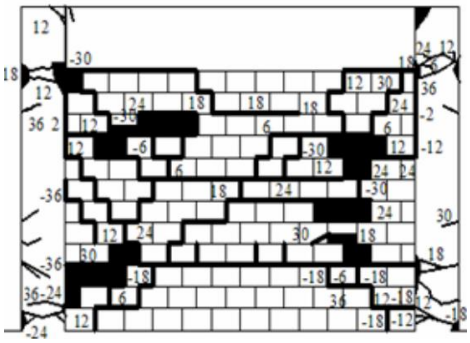

(b)

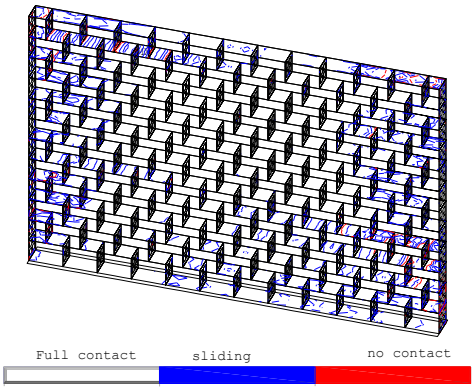

(c)

Fig. 14 Experimental and numerical crack patterns for specimen S: (a) numerical smeared crack patterns (cracks for plane *xz* in red; cracks for plane *xy* in blue; cracks for plane *yz* in purple-*z* is the vertical direction and the plane *xz* is the one represented in the figure), (b) experimental crack patterns, (c) status of the contact elements

material conditions are found.

For completeness, Fig. 14 provides a comparison between the crack patterns obtained from the experimental data and from the numerical analysis for specimen S. Figure 14(a) shows the numerical smeared crack pattern which can be compared with the experimental one shown in Fig. 14(b), while Fig. 14(c) shows the status of the contact elements to see that discrete cracks occur between the masonry courses. As can be seen, the numerical model reasonably captures the global crack pattern of the physical specimen and the separation between masonry courses. However, the numerical model overestimates the crack propagation in some parts of the infill panel. Given the lack of detailed experimental data, is it difficult to determine the reasons for such differences They may originate from numerical issues, such as the difficulty of capturing cyclic degradation effects or the fact that material properties are considered to be uniform across the model when in fact they might not be in the real specimen. Even though several hypothetical reasons could be presented, none can be thoroughly checked without detailed experimental data. Nevertheless, as referred for specimen M2, simulating experimental tests in scenarios where there is a certain

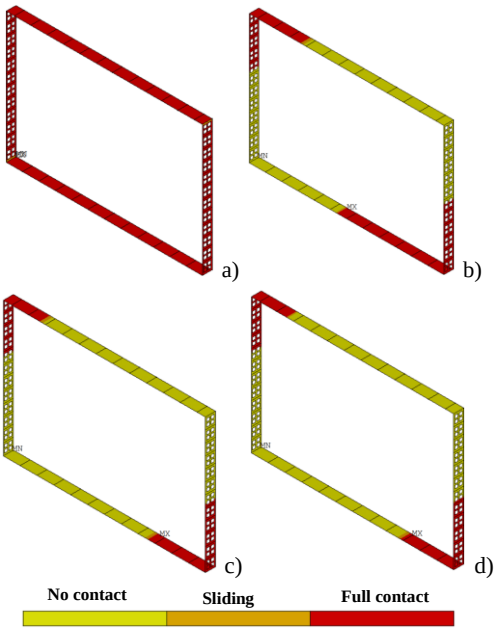

Fig. 15 The boundary contact status for specimen *S* at different levels of lateral drift: (a) 0.01%, (b) 0.10%, (c) 0.20% and (d) 0.40%

Table 3 Characteristics of the test specimens with partially infilled RC frames (Kakaletsis *et al*. 2008, Kakaletsis *et al*. 2009, Kakaletsis 2009)

Ratio	S	M2
Difference in the numerical maximum lateral force with respect to the corresponding experimental lateral force (%)	5.6	14.4
Maximum difference in the numerical lateral force with respect to the corresponding experimental lateral force (%)	15.8	38.6

Table 4 Lateral force differences between experimental and numerical results for the partially infilled specimens

Specimen	*a*	*b*
DO2	5.2	23.7
DX1	2.1	21.8
DX2	5.3	18.9
WO2	1.7	21.2
WO3	3.5	15.2
WO4	8.0	18.0
WX1	6.2	15.7
WX2	3.5	18.8

where:
a-Difference in the numerical maximum lateral force with respect to the corresponding experimental lateral force (%)
b-Maximum difference in the numerical lateral force with respect to the corresponding experimental lateral force (%)

amount of uncertainty regarding the as-built conditions of the specimens highlights the performance of the numerical model when reasonable assumptions are made regarding the main parameters that are involved.

Given these results, the proposed modelling approach is seen to provide a useful alternative to experimental tests since it is able to capture adequately the global behaviour envelope in terms of strength and stiffness. Additionally, this type of analysis also provides important information regarding the contact length between the infill panel and the RC frame (Fig. 15), which can be used to calibrate the parameters of an equivalent diagonal strut model (i.e., the effective width of the strut). As can be seen from Fig. 15, the interaction between the infill panel and the RC frame is inversely proportional to the drift ratio. Furthermore, it can also be seen that the RC frame loses most of the contact length with the infill panel for low levels of drift. In order to summarize these results, Table 3 presents the absolute differences observed between the numerical models and the

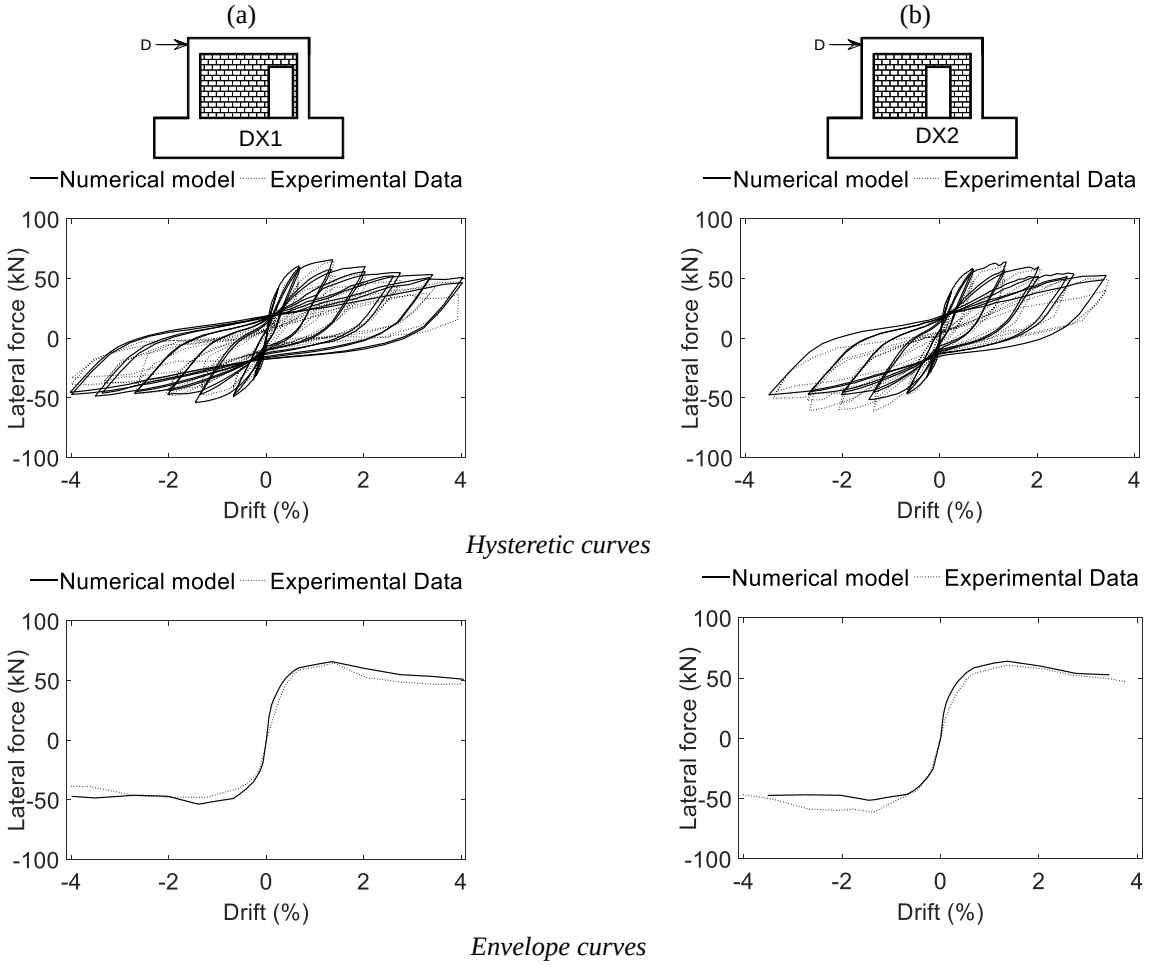

Fig. 16 Load-deflection curves obtained from the experimental tests and from the numerical models: (a) specimen DX1 (b) specimen DX2

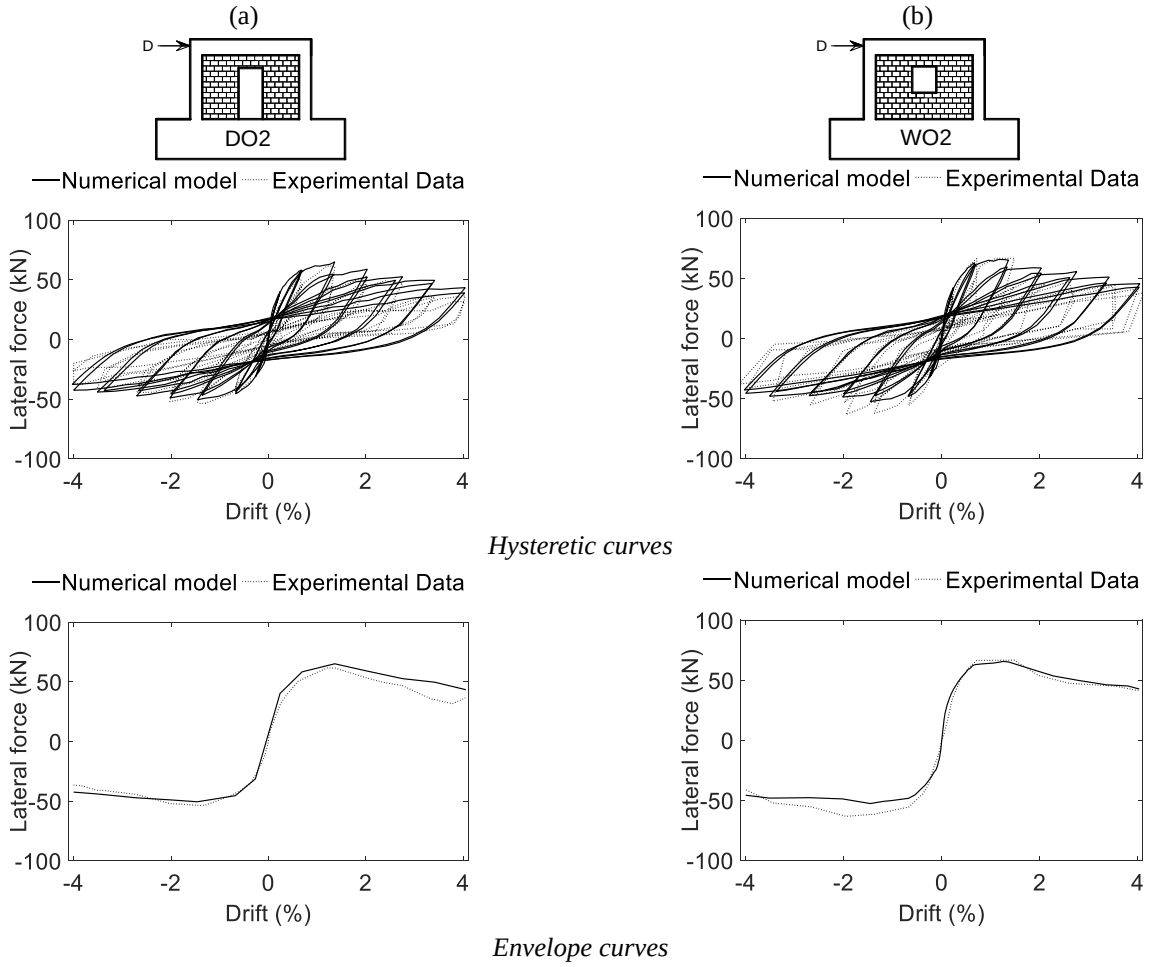

Fig. 17 (continued) Load–deflection curves obtained from the experimental tests and from the numerical models: (a) specimen DO2 (b) specimen WO2

experimental data. Differences in terms of the maximum lateral force and the maximum vertical difference (i.e., maximum difference in terms of lateral force for the same displacement) between the two curves are reported.

4.3 Analysis of the RC infilled frames with openings

Eight experimental tests on specimens with partially infilled RC frames were simulated using the developed numerical modelling strategy: three models with a door opening (the door is always the same size but at different locations), and five models with a window opening (the window changes in size and location). To analyse the performance of the numerical model, Figs. 16-19 compare the experimental and numerical lateral load-deflection curves of the specimens. As for the previous cases, the lateral deflection is represented in terms of drifts and both the full cyclic lateral load-deflection curves and the overall envelope curves are shown. As for the previous cases, the results indicate there is a good match between the experimental and the numerical behaviour curves, namely in terms of the global envelope representing the strength and stiffness evolution. Furthermore, the differences between the fully infilled frames (Fig. 13) and the partially infilled frames in terms of lateral stiffness and maximum strength is also clearly captured by the proposed numerical modelling approach. Still, differences between the unloading and reloading stiffnesses of the numerical and experimental results are also noticeable as results of factors previously referred. As for the previous case, Table 4 summarizes the results by presenting the absolute differences recorded between the numerical models and the experimental data. Differences reported are in terms of the maximum lateral force and the maximum vertical difference between the two curves.

5. Conclusions

In cases where experimental data are not available and experimental tests are unable to be carried out, numerical simulations using detailed FE models capable of representing the behaviour of RC masonry-infilled structures can be used as a proxy for the experimental testing. In this context, a detailed modelling approach was developed in the software ANSYS to simulate the behaviour of RC masonry-infilled frames under in-plane monotonic or cyclic loading with adequate accuracy and an affordable computational effort. To test the reliability of the proposed modelling approach, several examples of RC

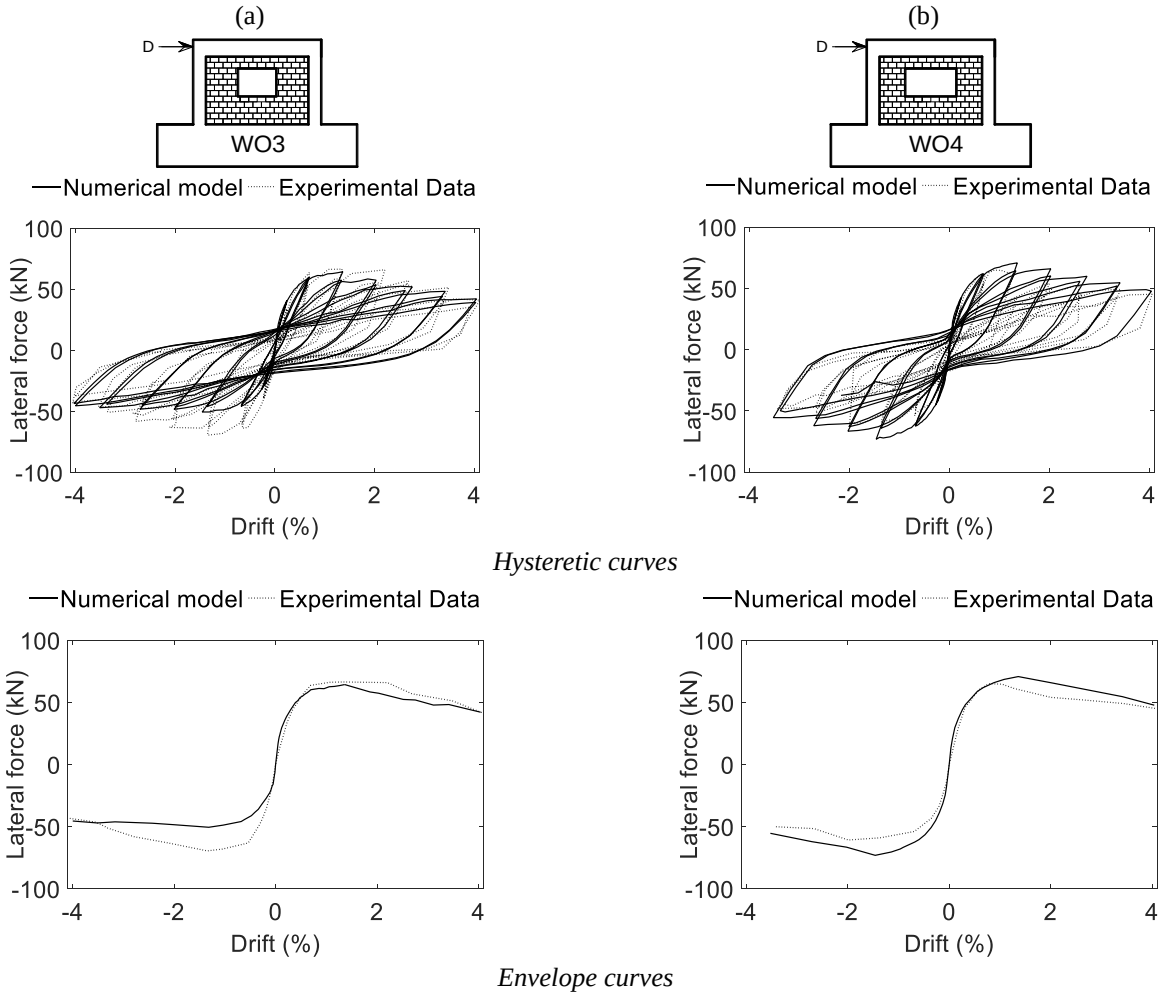

Fig. 18 Load–deflection curves obtained from the experimental tests and from the numerical models: (a) specimen WO3 and (b) specimen WO4

infilled frames with different infill configurations subjected to cyclic loading were analysed.

The results show that the detailed modelling approach is able to represent the behaviour of masonry infilled RC frames adequately and can be used to simulate this type of structural system using only the essential mechanical properties of the materials involved (i.e., without the need to test an entire specimen). This conclusion is supported by the ability of the model to adequately account for the more common masonry failure mechanisms, as well as to represent the strength and stiffness envelopes with a reasonable accuracy when compared to experimental results.

Finally, it is also referred that the duration of each analysis was between 60 to 72 hours, running on a PC with an Intel i7-4770K CPU. This computational cost is seen to be affordable given the reliability of the results that are obtained that allow calibrating simplified models more suited for probabilistic performance based earthquake engineering applications. In the overall, the proposed modelling approach is therefore seen to be a potential alternative to experimental testing.

Acknowledgements

The financial support provided by the Erasmus Mundus programme Al Fihri (ALFI1201678 grant) to the first author is gratefully acknowledged. The authors are also gratefully acknowledged to Professor Kakaletsis J. Demetrios (Technological Educational Institution of Serres, Serres) and Professor Christos G. Karayannis (University of Thrace, Xanthi, Greece) for kindly providing experimental and modelling data for the calibration and verification of the models. Authors also acknowledge the financial support of Project POCI-01-0145-FEDER-007457-CONSTRUCT-Institute of R&D In Structures and Construction funded by FEDER funds through COMPETE2020-Programa Operacional Competitividade e Internacionalização (POCI) -and by national funds through FCT-Fundação para a Ciência e a Tecnologia.

References

Alam, M., Nehdi, M. and Amanat, K. (2009), "Modelling and analysis of retrofitted and un-retrofitted masonry-infilled RC

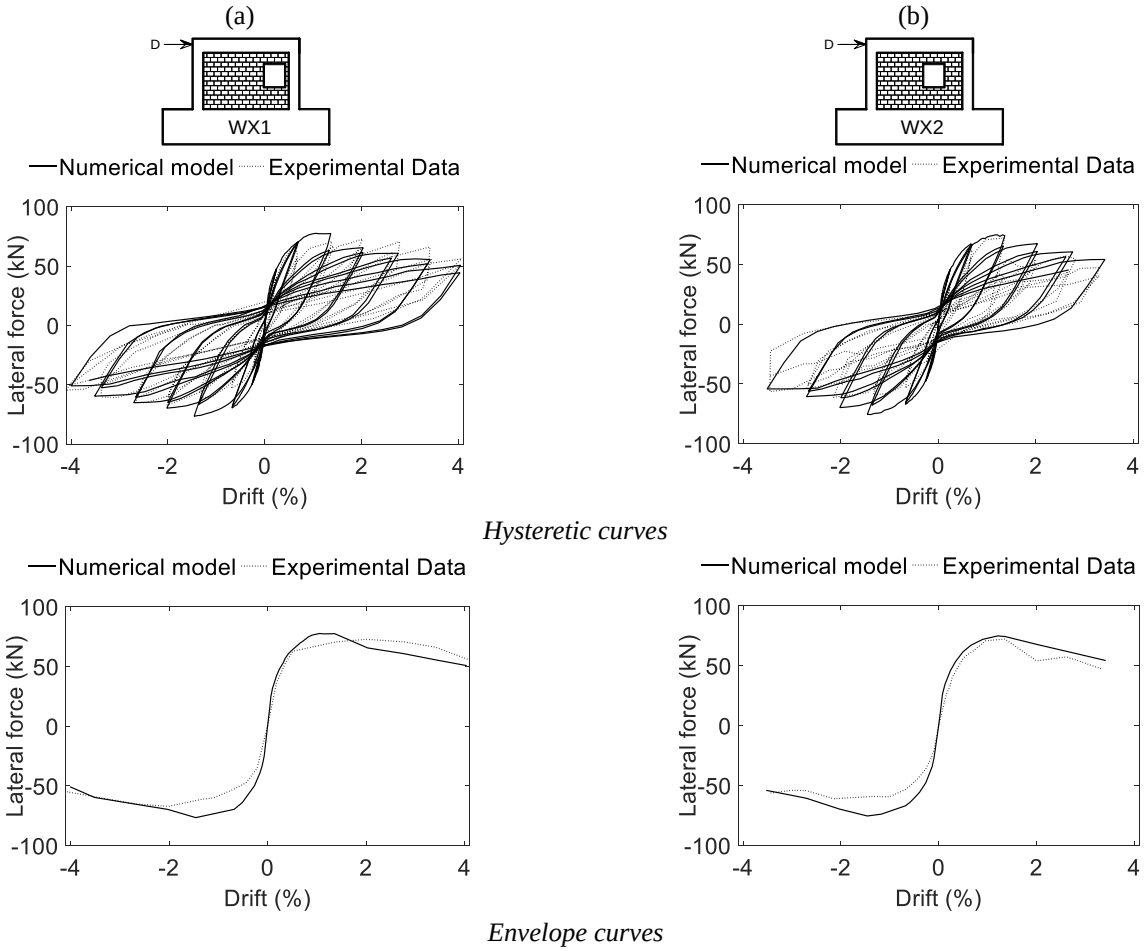

Fig. 19 Load-deflection curves obtained from the numerical models along with the experimental data for specimens with eccentric window openings: (a) specimen WX1 and (b) specimen WX2

frames under in-plane lateral loading", *Struct. Infrastr. Eng.*, **5**(2), 71-90.

Alfano, G. and Crisfield, M. (2001), "Finite element interface models for the delamination analysis of laminated composites: Mechanical and computational issues", *Int. J. Numer. Meth. Eng.*, **50**(7), 1701-1736.

Angel, R. (1994), "Behavior of reinforced concrete frames with masonry infill walls", PhD Thesis, University of Illinois, Champaign, USA.

ANSYS (2012), Theory Reference for the Mechanical APDL and Mechanical Applications Release 14.5, ANSYS Inc. Company, Release 14.5,Canonsburg, PA, USA.

Anthoine, A. (1992), "In-plane behaviour of masonry: A literature review", Commission of the European Communities, Joint Research Centre, Institute for Safety Technology, Ispra, Italy.

Asteris, P., Cotsovos, D., Chrysostomou, C., Mohebkhah, A. and Al-Chaar, G. (2013) "Mathematical micromodeling of infilled frames: State of the art", *Eng. Struct.*, **56**, 1905-1921.

Baker, J.W. (2015), "Efficient analytical fragility function fitting using dynamic structural analysis", *Earthq. Spectra*, **31**(1), 579-599.

Chansawat, K., Kachlakev, D., Miller, T. and Yim, S. (2001), "Fe modeling and experimental verification of an frp strengthened bridge", *Sem Annual Conference on Experimental and Applied Mechanics*, Portland, Oregon, USA.

Chen, X. and Liu, Y. (2016), "A finite element study of the effect of vertical loading on the in-plane behavior of concrete masonry infills bounded by steel frames", *Eng. Struct.*, **117**, 118-129.

Crisafulli, F. (1997), "Seismic behaviour of reinforced concrete structures with masonry infills", PhD Thesis, University of Canterbury, Christchurch, New Zealand.

De Luca, F., Verderame, G.M., Gómez-Martínez, F. and Pérez-García, A. (2014), "The structural role played by masonry infills on RC building performances after the 2011 lorca, spain, earthquake", *Bull. Earthq. Eng.*, **12**(5), 1999-2026.

DIANA (2011), "Finite element analysis: User's manual", TNO Building and Construction Research, Finite Element Analysis, Delft, Netherlands.

El-Dakhakhni, W.W., Elgaaly, M. and Hamid, A.A. (2003), "Three-strut model for concrete masonry-infilled steel frames", *J. Struct. Eng.*, **129**(2), 69-77.

Hendry, A. (1990), *Structural Masonry*, Scholium International, Macmillan Education Ltd, London, UK.

Hu, J., Chen, B., Smith, D., Flewitt, P. and Cocks, A. (2016), "On the evaluation of the bauschinger effect in an austenitic stainless steel-the role of multi-scale residual stresses", *Int. J. Plast.*, **84**, 203-223.

Ibrahim, Y.E. and El-Shami, M.M. (2011), "Seismic fragility curves for mid-rise reinforced concrete frames in kingdom of saudi arabia", *Ies J. Part A: Civil Struct. Eng.*, **4**(4), 213-223.

Induprabha, S. and Dilrukshi, K. (2011), "Contribution to numerical modelling of concrete-masonry interface in concrete framed structures with masonry infill", *International Conference on Structural Engineering Construction and*

Management, Kandy, Central, Sri Lanka

Kakaletsis, D. and Karayannis, C. (2008), "Influence of masonry strength and openings on infilled r/c frames under cycling loading", *J. Earthq. Eng.*, **12**(2), 197-221.

Kakaletsis, D. and Karayannis, C. (2009), "Experimental investigation of infilled reinforced concrete frames with openings", *ACI Struct. J.*, **106**(2), 132-141.

Kakaletsis, D.J. (2009), "Masonry infills with window openings and influence on reinforced concrete frame constructions", *Earthq. Resist. Eng. Struct. VII*, **104**, 445-455.

Kent, D.C. and Park, R. (1971), "Flexural members with confined concrete", *J. Struct. Div.*, **97**(7), 1969-1990.

Koutromanos, I., Stavridis, A., Shing, P.B. and Willam, K. (2011), "Numerical modeling of masonry-infilled RC frames subjected to seismic loads", *Comput. Struct.*, **89**(11), 1026-1037.

Kwan, A., Dai, H. and Cheung, Y. (1999), "Non-linear seismic response of reinforced concrete slit shear walls", *J. Sound Vib.*, **226**(4), 701-718.

Lourenço, P. and Rots, J. (1997), "Multisurface interface model for analysis of masonry structures", *J. Eng. Mech.*, **123**(7), 660-668.

Lourenço, P.B., Barros, J.O. and Oliveira, J.T. (2004) "Shear testing of stack bonded masonry", *Constr. Build. Mater.*, **18**(2), 125-132.

Mehrabi, A. and Shing, P. (1997), "Finite element modeling of masonry-infilled RC frames", *J. Struct. Eng.*, **123**(5), 604-613.

Mises, R.V. (1913), "Mechanics of solid bodies in the plastically-deformable state", *Nachrichten Von Der Gesellschaft Der Wissenschaften Zu Gottingen. Mathematisch-Physikalische Klasse*, **1**, 582-592.

Mohamed, H. (2017), "Seismic risk assessment of reinforced concrete frames with masonry infill", PhD Thesis, Faculty of Engineering of the University of Porto, Porto, Portugal.

Mohyeddin, A., Goldsworthy, H.M. and Gad, E.F. (2013a), "Fe modelling of RC frames with masonry infill panels under in-plane and out-of-plane loading", *Eng. Struct.*, **51**(1), 73-87.

Mohyeddin, A., Goldsworthy, H.M. and Gad, E.F. (2013b), "Sensitivity analysis of nonlinear behaviour of infill-frames under in-plane and out-of-plane loading", *Adv. Struct. Eng.*, **16**(10), 1729-1748.

Noorfard, R. and Marefat, S. (2009), "Finite element modelling and investigation of the effects of masonry infills on the behaviour of reinforced concrete (RC) frames", *3rd International Conference on Concrete and Development*, Tehran, Iran.

Pires, F.M.G. (1990), "Influence of masonry walls over the behavior of reinforced concrete frames under horizontal actions", PhD Thesis, National Laboratory for Civil Engineering Lisbon.

Ricci, P., De Luca, F. and Verderame, G.M. (2011), "6th april 2009 l'aquila earthquake, italy: Reinforced concrete building performance", *Bull. Earthq. Eng.*, **9**(1), 285-305.

Sattar, S. (2013), "Influence of masonry infill walls and other building characteristics on seismic collapse of concrete frame buildings", PhD Thesis, University of Colorado Boulder, Colorado, USA

Scott, B., Park, R. and Priestley, M. (1982), "Stress-strain behavior of concrete confined by overlapping hoops at low and high strain rates", *ACI Struct. J.*, **79**(1), 13-27.

Sezen, H., Whittaker, A., Elwood, K. and Mosalam, K. (2003), "Performance of reinforced concrete buildings during the august 17, 1999 kocaeli, turkey earthquake, and seismic design and construction practise in turkey", *Eng. Struct.*, **25**(1), 103-114.

Shing, P.B. and Mehrabi, A.B. (2002), "Behaviour and analysis of masonry-infilled frames", *Prog. Struct. Eng. Mater.*, **4**(3), 320-331.

Stavridis, A. and Shing, P. (2010), "Finite-element modeling of nonlinear behavior of masonry-infilled RC frames", *J. Struct. Eng.*, **136**(3), 285-296.

Tapan, M., Comert, M., Demir, C., Sayan, Y., Orakcal, K. and Ilki, A. (2013), "Failures of structures during the october 23, 2011 tabanlı (van) and november 9, 2011 edremit (van) earthquakes in turkey", *Eng. Fail. Anal.*, **34**, 606-628.

Tarque, N., Candido, L., Camata, G. and Spacone, E. (2015), "Masonry infilled frame structures: State-of-the-art review of numerical modelling", *Earthq. Struct.*, **8**(1), 225-251.

Taucer, F., Spacone, E. and Filippou, F.C. (1991), "A fiber beam-column element for seismic response analysis of reinforced concrete structures", Earthquake Engineering Research Center, College of Engineering, University of California, California, USA.

Uva, G., Raffaele, D., Porco, F. and Fiore, A. (2012), "On the role of equivalent strut models in the seismic assessment of infilled RC buildings", *Eng. Struct.*, **42**, 83-94.

Vamvatsikos, D. and Cornell, C.A. (2002), "Incremental dynamic analysis", *Earthq. Eng. Struct. Dyn.*, **31**(3), 491-514.

Vijaya, S., Shivakumaraswamy, B. and Ravikiran, K. (2014), "Numerical modelling on behaviour of reinforced concrete exterior beam-column joint retrofitte with externally bonded fiber reinforced polymere (frp)", *Ijret: Int. J. Res. Eng. Technol.*, **3**(6), 247-252.

Wael, W. and Drysdale, G. (2004), "3-d finite element modelling of masonry-infilled frames with and without openings", *13th International Brick and Block Masonry Conference*, Amsterdam, Netherlands.

William, K.J. and Warnke, E.D. (1975), "Constitutive model for the triaxial behavior of concrete", *Proceedings of the Int. Association for Bridge and Structural Engineering*, Ismes, **19**, 174.

Xiaohan, W. and Xilin, L. (1996), "Nonlinear finite element analysis of reinforced concrete slit shear wall under cyclic loading", *Journal of Tongji University*, 24(2), 117-123.

CC